

0-1* transition lies within $\Delta\nu$ of the laser frequency. All of those molecules will decay rapidly and nonradiatively to their 0* levels. It is important to observe that these 0* levels will subsequently fluoresce into a band which also¹⁰ has width $\Delta\nu_1^* + \Delta\nu_0^* \approx \Delta\nu_1^*$. Thus, simply by monitoring the 0*-0 fluorescence band, the width of the 1* vibrational level can be detected directly.

We expect, on the basis of our work with other molecules,^{8,9} that our conclusions regarding pentacene mixed crystals have fairly general relevance. If this is the case, then the elimination of inhomogeneous broadening by use of optical site-selection spectroscopy will be generally possible, greatly facilitating studies of homogeneous effects such as electron-phonon interactions and vibrational anharmonicities in organic mixed-crystal systems. Even more important will be the immediate improvement possible in measured limits on radiative and nonradiative vibrational lifetimes in large molecules.

Finally we point out an interesting and unexplained distinction between these and earlier results, obtained for tetracene⁸ and several other large organic molecules including pentacene.⁹ In the previous measurements the subject molecules were in vitreous, not crystalline, hosts but held at liquid-helium temperatures in all cases. The sharpest of these lines, with inhomogeneous broadening removed by the optical site-selection technique, still were about 1 cm⁻¹ wide.

In a vitreous host a subject molecule experiences a far greater broadening due simply to environmental irregularities than does a molecule in a crystal, but the limit of fluorescence line narrowing due to excitation by a very narrow-line laser should be the same in the two cases. That is, if the original line is an inhomogeneously broadened envelope of very narrow homogeneously broadened lines, then the homogeneous linewidth provides a lower limit on the extent of possible line narrowing, independent of the degree of inhomogeneous broadening in the original line. The discrepancy between the line-narrowing limit of 0.034 cm⁻¹ reported here for mixed crystals, and the limit of about 1 cm⁻¹ reported earlier for molecules in vitreous hosts, suggests that even at liquid-helium temperatures the vitreous hosts contribute an unexpected *homogeneous* component of width about 1 cm⁻¹ to the subject molecules' total spectral width. It will be very interesting to have optical site-selection results for similar molecules in Shpol'skii matrices, hosts that are intermediate between glasses

and crystals.¹¹

We wish to thank Dr. D. Ham of the University of Rochester Laboratory for Laser Energetics for the generous loan of the scanning Fabry-Perot interferometer. We thank I. D. Abella and A. L. Schawlow for several interesting discussions.

*Research partially supported by the U. S. Army Research Office (Durham).

¹B. Meyer, *Low Temperature Spectroscopy* (American Elsevier, New York, 1971), pp. 52-56.

²D. S. McClure, *J. Chem. Phys.* **22**, 1668 (1954).

³Unfortunately the mixed-crystal technique works relatively rarely for large organic molecules because of the great difficulties in finding suitable crystalline hosts. Ionic atomic mixed crystals are common, of course, and studies of low-temperature, sharp lines with inhomogeneous widths ~ 1 cm⁻¹ are by now well known [for an early example, see A. L. Schawlow, *J. Appl. Phys.*, Suppl. **33**, 395 (1962)]. Photon-echo work [see N. A. Kurnit *et al.*, in *Physics of Quantum Electronics*, edited by P. L. Kelley *et al.* (McGraw-Hill, New York, 1966), p. 267] provided the first experimental access to underlying homogeneous widths. More recent work, using direct narrow-line laser excitation is due to A. Szabo, *Phys. Rev. Lett.* **25**, 924 (1970), and **27**, 323 (1971).

⁴A preliminary investigation of residual inhomogeneous broadening in molecular Shpol'skii spectra has recently been reported: I. Abram, R. A. Auerbach, R. R. Birge, B. E. Kohler, and J. M. Stevenson, *J. Chem. Phys.* **61**, 3857 (1974).

⁵See, for example, D. B. Fitchen, in *Physics of Color Centers*, edited by W. B. Fowler (Academic, New York, 1968), p. 309; K. K. Rebane, *Impurity Spectra of Solids* (Plenum, New York, 1970), pp. 141-145; J. L. Richards and S. A. Rice, *J. Chem. Phys.* **54**, 2014 (1971); and, more recently, R. M. Hochstrasser and P. N. Prasad, in *Excited States*, edited by E. C. Lim (Academic, New York, 1974), Vol. 1, pp. 114 and 119.

⁶J. H. Meyling and D. A. Wiersma, *Chem. Phys. Lett.* **20**, 383 (1973).

⁷R. I. Personov, E. I. Al'shits, and L. A. Bykovskaya, *Pis'ma Zh. Eksp. Teor. Fiz.* **15**, 609 (1972) [*JETP Lett.* **15**, 431 (1972)]; L. A. Bykovskaya, R. I. Personov, and B. M. Kharlmov, *Chem. Phys. Lett.* **27**, 80 (1974).

⁸J. H. Eberly, W. C. McColgin, K. Kawaoka, and A. P. Marchetti, *Nature (London)* **251**, 215 (1974).

⁹W. C. McColgin, Ph. D. dissertation, Department of Physics and Astronomy, University of Rochester, 1975 (unpublished).

¹⁰The width of the fluorescence band will be the same as the width $\Delta\nu_1^*$ only if there is perfect site coherence during the nonradiative 1*-0* decay. If there is not, the observed fluorescence width may be larger than $\Delta\nu_1^*$ because of spectral diffusion, due for example to

excitation-exchange scattering among the sites during the nonradiative process. Thus, in the present case, our measurement also puts a limit of about 0.2 nsec on the time for spectral diffusion in low-temperature pentacene.

¹¹Unfortunately, the Shpol'skii-matrix measurements reported by Kohler *et al.* (see Ref. 4), were instrument-limited, with resolution on the order of 0.4 cm^{-1} , not narrow enough to pin down the residual homogeneous width of the lines measured.

Detection of Optical Surface Guided Modes in Thin Graphite Films by High-Energy Electron Scattering*

C. H. Chen and J. Silcox†

School of Applied and Engineering Physics, Cornell University, Ithaca, New York 14853

(Received 16 January 1975)

High-angular-resolution ($\sim 8 \times 10^{-6}$ rad), high-energy (75 keV), electron scattering from graphite thin films demonstrates energy losses due to the excitation of optical surface guided modes. Measurements of the dispersion offer considerable support for the anisotropic dielectric constant proposed by Tosatti and Bassani.

In this Letter, we report the observation for the first time of peaks in characteristic electron energy-loss spectra which can be clearly identified with the excitation of guided surface waves in a thin-film specimen. Such waves can most readily be visualized as electromagnetic waves propagating in the thin film in a wave-guide fashion. These excitations are contained within the usual surface-plasmon formalism¹ and become significant at long wavelengths in thin films of materials in energy regimes where the dielectric constant is greater than unity. Thus in the neighborhood of a strong absorption edge, the surface excitations above the edge are of surface-plasmon nature [provided the dielectric constant becomes sufficiently negative, i.e. $\epsilon(\omega) < -1$], whereas below the edge they become guided surface waves. In the infrared, in materials where a strong absorption edge arises as a result of surface-phonon effects, the equivalent excitation to the surface plasmon at that edge is the surface polariton, whereas the guided-mode equivalent has been identified as a wavelike "bulk" mode.² In the present case we are concerned with a situation in which the basic physical cause of the absorption edge is a normal interband transition. However as the system in question, graphite, is anisotropic some complexities are introduced into this simple picture.

Specifically, we report high-angular-resolution, energy-loss data as a function of scattering angle θ for a specimen of graphite, 75 nm thick, tilted so that the *c* axis (normal to the specimen plane) makes an angle of 60° with the incident beam. We demonstrate the existence of three surface modes

in the energy range between 4 and 11 eV at the smallest scattering angles. At large angles a single peak corresponding to a volume excitation is observed. In between, the volume and surface terms in the scattering probability cancel each other—a corresponding gap is seen in the excitation spectrum. The volume peak occurs precisely at the point where disagreement arises between the electron energy-loss measurements of Zeppenfeld³ and the optical observations of Willis, Feuerbacher, and Fitton⁴ using photoemission and secondary-electron emission and Klucker, Skibowski, and Steinmann⁵ using reflectivity measurements with synchrotron radiation. The observations reported here resolve that discrepancy and offer evidence in favor of the dielectric constants proposed by Tosatti and Bassani.⁶ The interpretation demonstrates the necessity for a complete calculation of the energy-loss probabilities including both anisotropic dielectric constants and retardation.

The apparatus and techniques have been described previously.^{7,8} Briefly a Hitachi HU11A electron microscope is used to provide a 75-keV electron beam parallel to 8×10^{-6} rad incident on the specimen while lenses after the specimen are adjusted to provide a long effective camera length (~ 25 m). A Wien electron spectrometer mounted underneath the electron microscope provides the energy analysis with an energy resolution ~ 0.5 eV. The entrance slit to the spectrometer is placed over the central electron beam and allows the passage of electrons scattered at different angles to the incident beam. The spectrometer deflects electrons in a direction perpendicular to

the slit according to energy so that the result, recorded on a photographic plate, is a direct map of the scattered intensity as a function of the energy loss, ΔE ($\equiv \hbar\omega$), and scattering angle θ ($\equiv q_{\perp}\lambda/2\pi$, where q_{\perp} is the scattering vector perpendicular to the electron beam and λ is the electron wavelength). The optical density of the photographic plate is, to a good approximation, linear with incident electron intensity (provided saturation is not reached) so that the dark regions on the plate represent regions of high electron intensity. Precise locations of maxima are obtained by microdensitometry using a Joyce-Loebl Mark IIIC densitometer. Single-crystal graphite films with the c axis perpendicular to the film surface were obtained by cleaving Madagascar graphite flakes using Teflon tapes.

Figure 1 shows the spectrum—intensity (as represented by optical density) as a function of ΔE and q_{\perp} —recorded photographically for a graphite flake estimated as 75 nm thick and tilted to an angle of 60° with the incident beam in order to identify and enhance the intensity of surface modes.⁸ We note that this photograph is a positive copy of the plate used to record the original data. The spectrometer slit has been set perpendicular to the axis of tilt so that q_{\perp} lies in the plane defined by the incident beam and the normal of the specimen. Under such conditions, the excitation wave vector of a surface excitation q_s in the plane of the specimen is given by $q_s = (\omega/v) \sin 60^{\circ} \pm q_{\perp} \times \cos 60^{\circ}$, where v is the velocity of the incident electrons and the plus and minus signs refer to

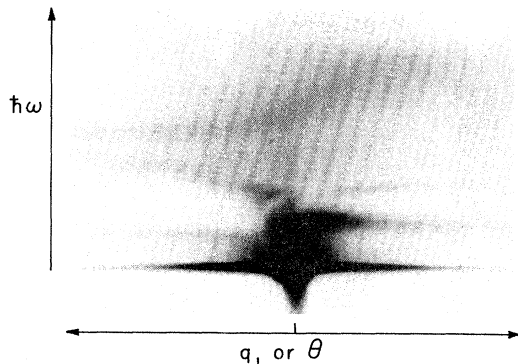


FIG. 1. Photograph of the scattered electron intensity $I(\Delta E, \theta)$ as a function of energy loss, ΔE , and scattering angle θ for thin graphite film (~ 75 nm thick) tilted at 60° . The degree of blackness is equivalent to intensity. The horizontal line at the bottom contains electrons scattered by elastic collisions and by phonons.

the scatterings occurring on each side of the incident beam. In Fig. 2 we have sketched the location of the intensity maxima (optical-density maxima) seen in Fig. 1 together with axes, units, and identification marks. The main features⁹ are in agreement with Zeppenfeld's earlier observations within the limits of his angular resolution and will be discussed elsewhere (see also Chen⁹). Particular features of interest here are the peak FG and the associated structure, not observed by Zeppenfeld, represented by dashed lines between E and F and reaching down to the origin. The peak FG shows little dispersion, is relatively sharp, and occurs at 11 eV. This is the peak observed by Zeppenfeld³ and not seen in the later work.^{4,5} We conclude therefore, in support of Zeppenfeld, that this peak quite definitely exists and that the measurements using photoemission, secondary-electron emission,⁴ and synchrotron radiation⁵ are insensitive to it. We now note that structure represented by the dashed lines between E and F has all the hallmarks of a surface-guided-mode dispersion pattern representing the excitation of three such modes.

In much thicker films than those under consideration here, the modes are identical with the trapped modes currently being exploited in optoelectronic devices.¹⁰ The dispersion relation for these modes is, however, contained within the surface-plasmon formalism.¹ Specifically for anisotropic materials, the attenuation coefficient α of the fields in a direction normal to the surface inside the slab is given by $\alpha = [\epsilon_{\perp}(q_s^2 - \epsilon_{\parallel}\omega^2/c^2)/\epsilon_{\parallel}]^{1/2}$, where $\epsilon_{\perp}(\omega)$ and $\epsilon_{\parallel}(\omega)$ are the two principal, complex, frequency-dependent dielectric

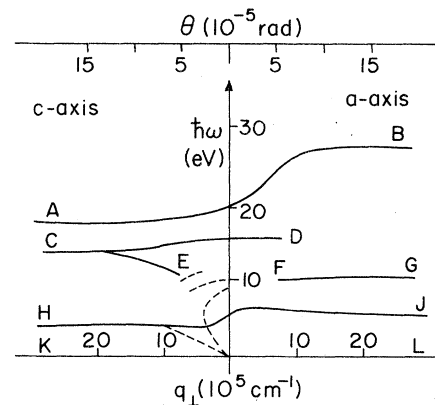


FIG. 2. Sketch of loss spectrum presented in Fig. 1. Solid curves represent the volume-type excitations and dashed curves the excitation of guided surface modes.

functions of the slab. α is a complex quantity in general. Depending on the particular behavior of $\epsilon_{\perp}(\omega)$ and $\epsilon_{\parallel}(\omega)$, α can be essentially real or imaginary. When α is essentially imaginary ($\alpha = i\beta$) the dispersion equations for p -polarized surface excitations take the guided-mode form

$$\begin{aligned} L^+ &= \alpha_0 \epsilon_{\perp} - \beta \tan \beta a = 0, \\ L^- &= \alpha_0 \epsilon_{\perp} + \beta \cot \beta a = 0. \end{aligned} \quad (1)$$

Here α_0 is the attenuation coefficient in the vacuum [$\epsilon(\omega) = 1$] and $2a$ is the thickness of the slab. The scattering probability has been evaluated for the uniaxial crystal slab and can be cast in a form (see Chen⁹) involving terms such as $\text{Im}(1/L^{\pm})$. We note that maxima in these functions, in general, occur at points given by dispersion equation (1). This is similar to the calculation for the isotropic case given by Kroger.¹

At this point, it is necessary to insert values for the dielectric constant. Two sets exist in the literature. Tosatti and Bassani⁶ (TB) derived one set from Zeppenfeld's data and Klucker, Skibowski, and Steinmann⁵ (KSS) derived another set from synchrotron-radiation data. We have evaluated the scattering probability using both sets and find that the TB data is an excellent fit. Figure 3

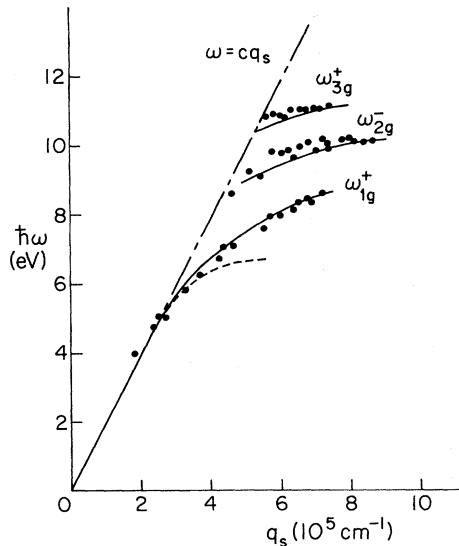


FIG. 3. Dispersion of the three guided modes shown in Fig. 1. Note that the data represented as a function of q_{\perp} in Fig. 1 have now been transformed to q_s , the wave vector in the surface of the specimen. Theoretical dispersion curves are calculated for a 75-nm-thick film using TB's data (represented by solid curves) and KSS's data (represented by dashed curve).

deals specifically with the guided-mode dispersion for a graphite film 75 nm thick. Note that the data represented as a function of q_{\perp} in Figs. 1 and 2 have now been transformed to q_s , the wave vector in the surface of the sample. The dots represent measurements taken from densitometer traces of the plate of Fig. 1 and the solid line represents the location of the calculated intensity maxima for the three lowest modes, ω_{1g}^+ , ω_{2g}^- , and ω_{3g}^+ . In this notation, the symmetry (+, -) relates back to expression (1) and the integers arise from the conditions $(m-1)\pi/2 < \beta a < m\pi/2$. The dashed line represents the only peak which arises in the calculation when the KSS data are used. Referring back to Fig. 2, calculations of the complete scattering probability including both surface and volume terms as a function of energy at various scattering vectors also demonstrate that the peak *FG* arises from volume terms and is enhanced considerably as a result of relativistic terms. It should therefore be considered as a Cherenkov-enhanced volume interband transition. The gap detected in Fig. 1 between the volume loss *FG* and the surface losses also arises in the calculations—essentially the volume and surface terms cancel each other out.

The primary difference between the two dielectric functions is a strong absorption peak at 11 eV in $\epsilon_{2\parallel}$ in the TB function. In order to explore the consequences of reducing the strength of this peak we have modeled the constants in the form $\epsilon(\omega) = 1 + \sum \omega_s^2 / (\omega_T^2 - \omega^2 + i\omega\gamma)$ (following Cazaux¹¹) with constants as given in the Table I. The interesting conclusion arising from calculations varying the strength of the 11-eV peak from the TB values to the KSS values is that the dispersion peaks, ω_g , are quite sensitive to the strength of that peak down to an energy of ~ 6 eV and that one

TABLE I. Values used to model the dielectric constant ϵ_{\perp} and ϵ_{\parallel} after Cazaux (Ref. 11).

	ω_s (eV)	ω_T (eV)	γ (eV)
ϵ_{\perp}	12.5	4	2.5
$\epsilon_{\parallel}^{TB}$	21.6	14	4.32
	12.5	16	6
$\epsilon_{\parallel}^{KSS}$	12.5	27.5	14.4
	5.5	11	1.5
	13	16	6
	12.5	27.5	14

should stay relatively close to the TB values.

Finally, we note that we have made observations on flakes of estimated thicknesses 50 nm showing two modes and 25 nm showing one mode—again as expected for the surface guided waves. We believe this is the first clear observation of these waves as a solid-state thin-film excitation. They do not occur in normal optical-reflectance data unless deliberate efforts are made to couple to them with a prism or grating. We have evidence for the excitation of such modes in a semiconductor Si and an insulator Al_2O_3 which will be published elsewhere. The experiment also demonstrates the value of high-energy electron-loss experiments in determining the anisotropic dielectric constant in this region. As pointed out by Abeles, Washburn, and Soonpaa,¹² very small errors in absolute reflectivity measurements can give rise to significant deviations in the optical constants, e.g., optical constants can vary by a factor of 100 for absolute reflectivity measurements good to 0.5%, whereas an accuracy of 0.03% results in an uncertainty of a factor of 2 in the optical constants. This may have occurred in the synchrotron-radiation measurements on graphite.⁵

*Work supported by Advanced Research Projects Agency through the Materials Science Center at Cornell University.

†Currently on sabbatical leave at Bell Telephone Laboratories, Murray Hill, N. J. 07974.

¹See, e.g., K. L. Kliewer and R. Fuchs, Phys. Rev.

114, 495 (1966); E. Kroger, Z. Phys. 235, 403 (1970).

²A. A. Maradudin, E. W. Montroll, G. H. Weiss, and I. P. Ipatova, *Theory of Lattice Dynamics in the Harmonic Approximation* (Academic, New York, 1971), pp. 550–555.

³K. Zeppenfeld, Z. Phys. 211, 391 (1968).

⁴R. F. Willis, B. Feuerbacher, and B. Fitton, Phys. Rev. 4, 2441 (1971).

⁵R. Klucker, M. Skibowski, and W. Steinmann, in *Proceedings of the Third International Conference on Vacuum Ultraviolet Radiation Physics, Tokyo, Japan, 1971* (The Physical Society of Japan, Tokyo, 1971), Paper 31 PA2.

⁶E. A. Tosatti and F. Bassani, Nuovo Cimento 65B, 161 (1970).

⁷G. H. Curtis and J. Silcox, Rev. Sci. Instrum. 42, 630 (1971); R. H. Wade and J. Silcox, Phys. Status Solidi 19, 57 (1967).

⁸R. Vincent and J. Silcox, Phys. Rev. Lett. 31, 1487 (1973)

⁹A. listing of the features of Figs. 1 and 2 follow [after Tosatti and Bassani, Ref. 5; and C. H. Chen, Ph.D. thesis, Cornell University, 1974 (unpublished), available as Cornell Materials Science Center Report No. 2302]. $A \rightarrow B$: $\sigma + \pi$ plasmon with \vec{q} ranging from the c axis (A , 19 eV) to the a axis (B , 27.5 eV). $H \rightarrow J$: mixture of $\pi \rightarrow \pi$ interband transitions at Q (H , 4.5 eV) and π plasmons (J , 6 eV). $K \rightarrow L$: thermal diffuse (phonon) scattering. CE is similar to FG . CD is somewhat uncertain but is presumably associated with the $\vec{E} \parallel c$ interband transition (14.5 eV) at P (Willis, Feuerbacher, and Fitton, Ref. 3).

¹⁰R. E. Collin, *Field Theory of Guided Waves* (McGraw Hill, New York, 1960), p. 470; D. Marcuse, *Light Transmission Optics* (Van Nostrand-Reinhold, New York, 1972).

¹¹J. Cazaux, Solid State Commun. 8, 545 (1970), and Opt. Commun. 2, 173 (1970).

¹²F. Abeles, H. A. Washburn, and H. H. Soonpaa, J. Opt. Soc. Am. 63, 104 (1973).

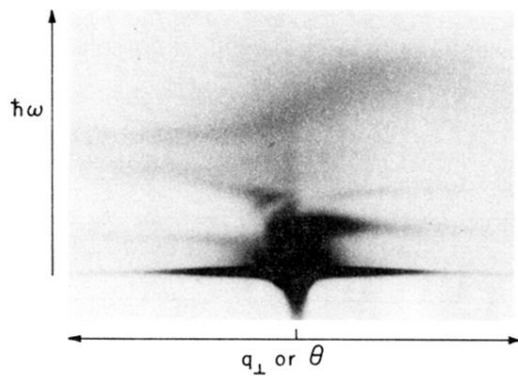


FIG. 1. Photograph of the scattered electron intensity $I(\Delta E, \theta)$ as a function of energy loss, ΔE , and scattering angle θ for thin graphite film (~ 75 nm thick) tilted at 60° . The degree of blackness is equivalent to intensity. The horizontal line at the bottom contains electrons scattered by elastic collisions and by phonons.